

Dynamics of Orientation Tuning in Macaque V1: The Role of Global and Tuned Suppression

Dario L. Ringach,¹ Michael J. Hawken,² and Robert Shapley²

¹*Departments of Neurobiology and Psychology, Jules Stein Eye Institute, Brain Research Institute, University of California, Los Angeles, California 90095; and* ²*Center for Neural Science, New York University, New York City, New York 10003*

Submitted 11 November 2002; accepted in final form 11 February 2003

Ringach, Dario, Michael J. Hawken, and Robert Shapley. Dynamics of orientation tuning in macaque V1: the role of global and tuned suppression. *J Neurophysiol* 90: 342–352, 2003. First published February 26, 2003; 10.1152/jn.01018.2002. The temporal development of neural selectivity to physical attributes of a visual stimulus, such as its orientation and spatial frequency, can provide important clues about mechanisms of cortical tuning. We measured the dynamics of orientation tuning in macaque primary visual cortex (V1) and found several dynamical features in the data: changes in global enhancement and suppression, narrowing of orientation bandwidth, small but significant shifts in preferred orientation, and “Mexican-hat” tuning curves. The dynamics data were analyzed with a model that sums two fixed, tuned components (enhancement and suppression) and one global (untuned) component. The analysis suggests that there is early global enhancement followed by global and tuned suppression. Tuned suppression accounts for the dynamical reduction of orientation bandwidth and for the generation of Mexican-hat tuning profiles. Our findings imply that global and tuned suppression are important factors that determine the selectivity and dynamics of V1 responses to orientation.

The temporal development of neural selectivity to stimulus attributes can provide important clues about the underlying circuitry (Bredfeldt and Ringach 2002; Pei et al. 1994; Ringach et al. 1997b; Volgushev et al. 1995). Cortical excitation and inhibition onto a neuron are expected to be delayed with respect to the monosynaptic input from the lateral geniculate nucleus (LGN). Suppose one measures responses of a cortical neuron at different delay times with respect to stimulus onset. The early response would be dominated by excitation from the LGN input, whereas the late response would correspond to a combination of both LGN input and intracortical interactions. For orientation-tuning dynamics, some groups report dynamical changes in the shape of the tuning curves (Pei et al. 1994; Ringach et al. 1997b; Volgushev et al. 1995) while others observe a scaling of its magnitude and no significant changes in its shape (Celebrini et al. 1993; Gillespie et al. 2001; Mazer et al. 2002; Muller et al. 2001; Sharon and Grinvald 2002).

In our earlier study (Ringach et al. 1997b) on the timing of the development of orientation tuning, we found that there were, in many cells, significant dynamical changes in shape of the orientation tuning curves. In particular, we suggested that the development of Mexican-hat tuning curves in the response could be accounted for by the presence of a tuned suppressive

component centered on the preferred orientation of the cell. In more recent studies, we have concluded that in addition to a tuned suppressive component, there is a global suppressive component involved in the tuning for orientation and spatial frequency (Bredfeldt and Ringach 2002; Ringach et al. 2002a). However, up until now, we only reported results about these global components at a fixed delay time (the peak) in the time evolution of the response. In this paper, we bring together these concepts to study both the time evolution of the global components in the dynamical response and the relationship of the global to the tuned components. This brings new insights into the cortical processes that are responsible for the generation of orientation tuning.

Here we re-examine the dynamics of orientation tuning in macaque V1 using an improved version of the reverse-correlation method where in addition to oriented patterns, “blank” frames of uniform luminance appear within the stimulation sequence (Ringach et al. 1997a). The blanks provide a baseline that allows direct detection of response enhancement and suppression by an oriented pattern. This modified reverse-correlation technique allowed us for the first time to measure enhancement and suppression components that are un-tuned for orientation. Previous techniques used by us and others (Mazer et al. 2002) do not allow the measurement of such global effects of oriented dynamical stimuli. These new measurements reveal important new phenomena, as shown in detail in RESULTS. One new phenomenon is global response enhancement early in the response of most neurons. The second new phenomenon is global suppression, also observed in most neurons. What is remarkable is the rapid time course of global suppression and its strength. In many neurons, we also observed the phenomenon of orientation-tuned suppression that was evident in our earlier data (Ringach et al. 1997b). Because of the overlap in time of enhancement and suppression, we attempted to gauge the strength of the global and the tuned suppression relative to that of enhancement through analysis with a descriptive model.

The dynamics data were analyzed in the context of a model in which, at each time, the tuning curve is obtained as a linear combination of two fixed, tuned components (enhancement and suppression) and one global (untuned) component. Data analysis with this model suggests that early global enhance-

Address for reprint requests: D. L. Ringach, Dept. of Psychology, Franz Hall, University of California, Los Angeles, CA 90095-1563 (E-mail: dario@ucla.edu).

The costs of publication of this article were defrayed in part by the payment of page charges. The article must therefore be hereby marked “advertisement” in accordance with 18 U.S.C. Section 1734 solely to indicate this fact.

ment causes the cell to respond to all orientations. Then global and tuned suppression develop rapidly and are comparable in magnitude to the tuned enhancement the cells receive. The suppressive components appear responsible for increasing the “modulation depth” of the tuning curve, for the dynamical narrowing of orientation bandwidth, for the generation of Mexican-hat tuning profiles, and for producing small shifts in the preferred orientation over the time course of the response. This leads to the conclusion that global and tuned suppression are important factors that determine the selectivity and dynamics of V1 responses to orientation.

METHODS

Animal preparation and experimental protocol

Acute experiments were performed on adult Old-World monkeys (*Macaca fascicularis*) in compliance with National Institutes of Health and New York University/UCLA guidelines. Animal preparation and recording were done as described in Ringach et al. (2002a,b). Each cell was stimulated monocularly through the dominant eye and characterized by measuring its steady-state response to high contrast drifting gratings (the non-dominant eye was occluded). Using this method, we recorded basic attributes of the cell, including spatial and temporal frequency tuning, orientation tuning, and contrast and color sensitivity as well as area summation curves. Receptive fields were located at eccentricities between 1 and 6°. The mean luminance of the screen was 50 cd/m², the viewing distance 90–120 cm, and the refresh rate was 60 Hz or 100 Hz.

Reverse correlation in the orientation domain

A modified version of reverse correlation in the orientation domain was used to measure the time evolution of orientation tuning. For each cell, a set S of sinusoidal gratings of a fixed spatial frequency (optimal for the cell) and contrast (in the range 80–99%) but different orientations and spatial phases was generated and stored in the computer’s memory. The orientation domain was sampled in equal steps ranging from 3 to 12°. For most cells, the angular step was fixed at 10°. For each orientation, sinusoidal gratings at eight equally spaced spatial phases, spanning the entire 360° range, were included in the set. Eight “blank” (uniform) images, of the same luminance as the mean of the gratings’ luminance, were included in the set as well. In a typical experiment the total number of images in S was 152 (18 orientations times 8 spatial phases plus 8 blanks).

The stimulus was generated by randomly selecting, at each video refresh frame, a new image from S with replacement. The stimulus was presented in 30-s-long trials with ~1- to 2-s inter-stimulus intervals. A total of 30 trials was presented to each cell, making the total experimental time 15 min. The specific image sequence was saved by the computer, and action potentials were recorded and time-stamped by the data acquisition system. The radius of the stimulus was two to four times the radius of classical receptive field (RF) defined by the peak or saturation point of an area summation curve (Sceniak et al. 1999). Thus both the classical RF of the cell and its surround were stimulated. We reasoned that under these conditions both feed-forward and intracortical mechanisms of orientation tun-

ing may be engaged, while stimuli restricted to the classical receptive field may bias the results to the direct contribution of the LGN inputs. In addition, natural images are spatially extended and contours tend to have long-range structure. Large stimuli covering both the receptive field and the surround approximate the natural situation closer than a stimulus restricted to the classical receptive field of the neuron.

The time course of orientation tuning was determined according to the following algorithm. First, an array of counters corresponding each to the orientations present in the stimulus, and one separate counter representing the blanks, were zeroed. A fixed value of a time-delay parameter τ was selected. For each nerve impulse, we went back τ ms and determined the frame that was last present in the image sequence. If the stimulus was a grating, the counter corresponding to its orientation was incremented by one. If the stimulus was a blank, the counter corresponding to the blanks was incremented by one. Gratings of different spatial phases but the same orientation contributed to the same counter. Thus this procedure averages across spatial phase at each orientation. At the end of this procedure, all the spikes recorded end up being distributed in the counters. Thus the sum of all the counts in the counters equal the total number of spikes collected. This is the case *irrespective* of the time delay chosen. The resulting counts were normalized by the actual number of times each orientation (or blank) appeared in the sequence. This provides an estimate of the probability that the cell will fire in a window (τ , $\tau + T$) ms after a stimulus is shown (where T is the duration of 1 frame). This function is identical, up to a scaling factor, to the probability that a stimulus preceded a spike by τ ms. In previous work, we described our results in terms of the probability of a stimulus *preceding* a spike; but in recent years, we realized that our colleagues find it more intuitive to think about the “forward” interpretation, which we now adopt. These two interpretations are equivalent if the “forward” cross-correlation is smoothed in time with a T -ms box window. Once the probability of firing in response to an oriented pattern, $p(\theta, \tau)$, and the blank, $p(\text{blank}, \tau)$, were estimated we calculated $R(\theta, \tau) = \log_{10}[p(\theta, \tau)/p(\text{blank}, \tau)]$, which we refer to as the tuning curve at a time lag τ . Oriented patterns that generate responses identical to the “blank” are mapped to $R(\theta, \tau) = 0$, stimuli that enhance cell’s response are mapped to $R(\theta, \tau) > 0$, while stimuli that suppress the cell’s response are mapped to $R(\theta, \tau) < 0$. A statistical justification for the log transform in the definition of $R(\theta, \tau)$ was provided in Ringach et al. (2002a). Furthermore, one can view this transformation as providing an estimation of a log-linear model of $p(\theta, \tau)$ based on the stimuli assuming that the weight of the “blank” stimulus is zero. A log-linear model for the probability of firing is more appropriate than simply linear regression as the latter can generate predictions outside the [0, 1] range.

Nonparametric analysis of orientation dynamics

Consider a hypothetical tuning curve at a fixed time lag (Fig. 1). Using nonparametric methods, we estimate a number of features of the curve. These include the orientation angle of the peak response, θ_{\max} , and its magnitude R_{\max} ; the orientation angle and magnitude of the minimum response, θ_{\min} and R_{\min} ; the angle orthogonal to θ_{\max} , denoted here by θ_{orth} , and the magnitude attained by the tuning curve there, R_{orth} ; the “mod-

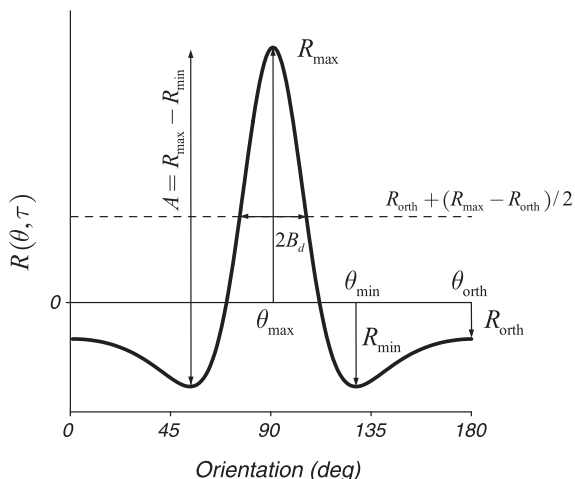


FIG. 1. Shape analysis of $R(\theta, \tau)$. The curve illustrates an orientation tuning curve at a fixed value of τ and several parameters extracted to analyze its shape. We measured the orientation angle of the peak response, θ_{\max} , and its magnitude R_{\max} ; the orientation angle and magnitude of the minimum response, θ_{\min} and R_{\min} ; the angle orthogonal to θ_{\max} , denoted here by θ_{orth} , and the magnitude attained by the tuning curve there by R_{orth} ; the “modulation depth” of the response, defined by $A = R_{\max} - R_{\min}$; and the dynamic half-bandwidth B_d defined by half the width of the tuning curve at a criterion level of $R_{\text{orth}} + (R_{\max} - R_{\text{orth}})/2$.

ulation depth” of the tuning curve, defined by $A = R_{\max} - R_{\min}$; and the dynamic half-bandwidth B_d defined by half the width of the tuning curve at a criterion level of $R_{\text{orth}} + (R_{\max} - R_{\text{orth}})/2$.

Parametric analysis

The parametric analysis was performed by fitting $R(\theta, \tau) = \alpha(\tau)E(\theta) + \beta(\tau)S(\theta) + \gamma(\tau)$ to the data, where

$$E(\theta) = \frac{\exp(\kappa_e \cos(2(\theta - \theta_e))) - \exp(-\kappa_e)}{(\exp(\kappa_e) - \exp(-\kappa_e))}$$

is a von Mises “distribution” (Mardia, 1972) normalized between zero and one. The von Mises distribution has been shown to provide very good fits to empirical data (Swindale 1998). The parameter θ_e determines the center of the component and κ_e its width. Similarly, the suppressive component was parameterized by

$$S(\theta) = \frac{\exp(\kappa_s \cos(2(\theta - \theta_s))) - \exp(-\kappa_s)}{(\exp(\kappa_s) - \exp(-\kappa_s))}$$

The centers of the two tuned components are not constrained to be equal. This allows the model to fit asymmetric tuning curves as well. Fitting of $R(\theta, \tau)$ was done by a fixed-point algorithm defined by the repeated interaction of two steps. In the first step, we assumed the parameters of $E(\theta)$ and $S(\theta)$ were known (and fixed) and found the best fitting coefficients at each time delay independently (under the constraints $\alpha, \beta > 0$). In the second step, we found the best fitting values of $(\theta_e, \kappa_e, \theta_s, \kappa_s)$ using the coefficients from the first step. The process was repeated until there was $<0.1\%$ change in the parameters from one interaction to the next. Although we do not have a proof that this algorithm is guaranteed to converge in all situations, it worked remarkably well in nearly every single instance we tried.

Confidence intervals

Confidence intervals for the estimated parameters were determined by bootstrap simulation as follows (Efron and Tibshirani 1993). For each time delay, the algorithm provides a distribution of N spikes into M bins. These multinomial data were resampled to generate different tuning curves, and the parameters estimated from the resampled data. A total of 500 simulations was performed at τ_{dev} and τ_{dec} to determine 95% confidence intervals for each parameter and their differences. For each data set, nonparametric estimates were obtained after linearly interpolating the raw data with 0.1° resolution and smoothing the tuning curve with a von Mises distribution with a parameter $\kappa = 14$, which corresponds to a half-bandwidth at half-height of 10° .

RESULTS

Nonparametric analysis

The behavior of $A(\tau)$, $R_{\min}(\tau)$, and $R_{\text{orth}}(\tau)$ for four representative neurons is depicted in Fig. 2, *left*. The modulation depth, $A(\tau)$, normally increases to reach a peak and then declines back to baseline. We used the time course of the modulation depth to define three time lags at which the orientation tuning curves were subsequently analyzed (Fig. 2, *middle* and *right*). These correspond to the points at which the modulation depth achieved its maximum value (τ_{pk}), and the points at which it achieved half its maximum value during the development (τ_{dev}) and decay (τ_{dec}) phases of the response (vertical dashed lines in Fig. 2, *left*). The distribution of $\tau_{\text{dec}} - \tau_{\text{dev}}$ over the V1 population had a mean of 22.3 ± 6.6 ms (1 SD) and the dynamical changes described in the following text occur over this time scale.

Figure 2, *middle* and *right*, depicts orientation-tuning curves for these four representative neurons at τ_{dev} (red, *middle*), τ_{dec} (blue, *middle*), and τ_{pk} (*right*). The changes with time in the height of these curves compared to the baseline, and the changes in their shapes, show that orientation selectivity varies dynamically in most V1 neurons in a very clear way.

The dynamic behavior of $R_{\min}(\tau)$ shows a number of important features. In all four examples, $R_{\min}(\tau_{\text{dev}}) > 0$, as the red curves in Fig. 2, *middle*, are above zero for all four neurons. This means that during the development of the response *all* orientations induced the cell to fire more than to a blank stimulus. In contrast, $R_{\min}(\tau_{\text{dec}}) < 0$, indicated by the blue curves in Fig. 2, *middle*, being below zero. Thus during the decay phase of the response, some orientations suppressed spike firing. In some V1 neurons, this effect appears to be mediated by global suppression (Fig. 2, *A* and *B*, *middle* and *right*). In other cells, however, there is also evidence of tuned suppression developing over the time course of the response, which causes the shape of the tuning curve to develop into a Mexican-hat profile during the decay phase (Fig. 2, *C* and *D*). For the cells in Fig. 2, *C* and *D*, $R_{\min}(\tau)$ and $R_{\text{orth}}(\tau)$ begin to diverge around the time of the peak response, implying that after τ_{pk} the minimum response occurs at a location other than the orthogonal—the signature of a Mexican-hat profile.

Average dynamics in V1

The average dynamics of A , R_{\min} , and R_{orth} in our population of $n = 178$ V1 cells are shown in Fig. 3. An important feature

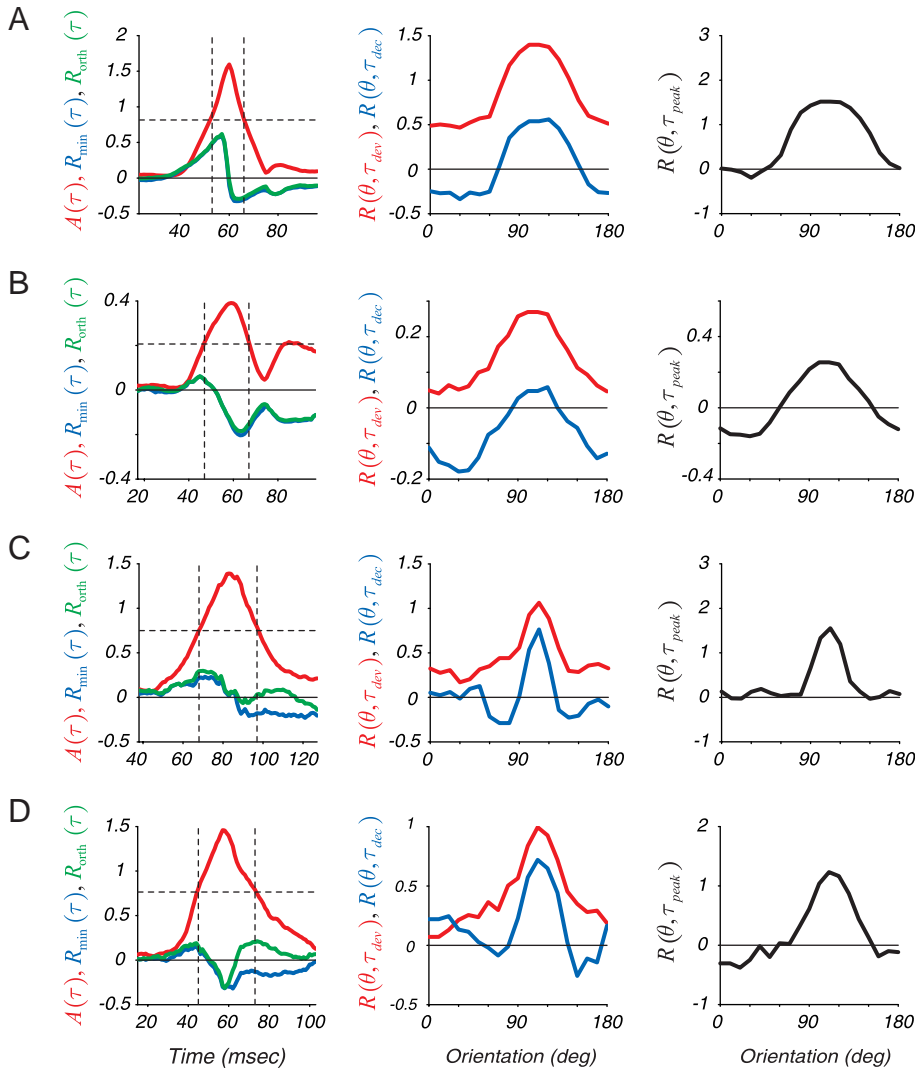


FIG. 2. Dynamics of orientation tuning in macaque V1 in 4 representative neurons. Each row represents a different cell. *Left*: the dynamics of $A(\tau)$ (red), $R_{\min}(\tau)$ (blue), and $R_{\text{orth}}(\tau)$ (green). In A and B, the green and blue curves are nearly identical. The horizontal dashed line represents the criterion level of $A(\tau_{\text{pk}})/2$, and the vertical dashed lines indicate τ_{dev} and τ_{dec} . *Middle*: $R(\theta, \tau_{\text{dev}})$ (red) and $R(\theta, \tau_{\text{dec}})$ (blue). To avoid clutter, $R(\theta, \tau_{\text{pk}})$ is shown *right*.

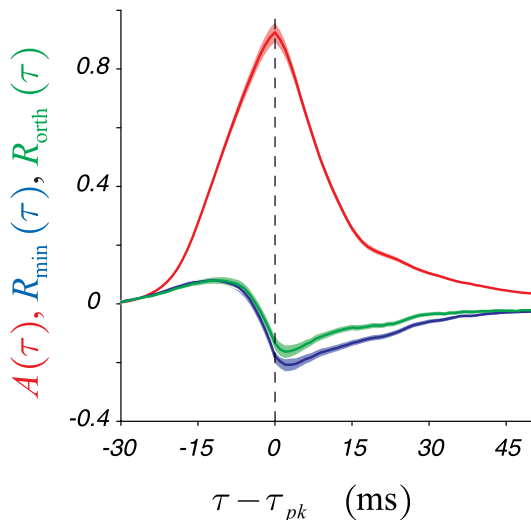


FIG. 3. Average dynamics of $A(\tau)$ (red), $R_{\min}(\tau)$ (blue), and $R_{\text{orth}}(\tau)$ (green) in the population of V1 neurons we studied ($n = 178$). Curves from different cells were aligned at τ_{pk} and averaged. Light shaded regions represent ± 1 SE.

of the data is the sharp downward change in time course of $R_{\min}(\tau)$ and $R_{\text{orth}}(\tau)$ before τ_{pk} . This suggests that the mechanism of suppression is rapid and contributes to the modulation depth at the peak time. Another important feature is the positive sign of R_{\min} and R_{orth} early in the response, indicating that, on average, V1 cells tend to respond to *all* orientations at this time.

Population analysis

The dynamics of R_{\min} across the population are analyzed in Fig. 4. There is an initial tendency for cells to respond to all orientations during the development phase of the tuning curve—the sample mean of $R_{\min}(\tau_{\text{dev}})$ is significantly greater than zero (t -test, $P < 3 \times 10^{-6}$; Fig. 4A, *bottom*). However, most cells tend to be suppressed at some orientations during response decay because the sample mean of $R_{\min}(\tau_{\text{dec}})$ is significantly less than zero (t -test, $P < 1 \times 10^{-10}$; Fig. 4, *left*). Thus R_{\min} decreases from the development to the decay phases of the response as illustrated by the difference histogram along the diagonal (Fig. 4A). The average difference $R_{\min}(\tau_{\text{dev}}) - R_{\min}(\tau_{\text{dec}})$ is significantly greater than zero (t -test, $P < 1 \times$

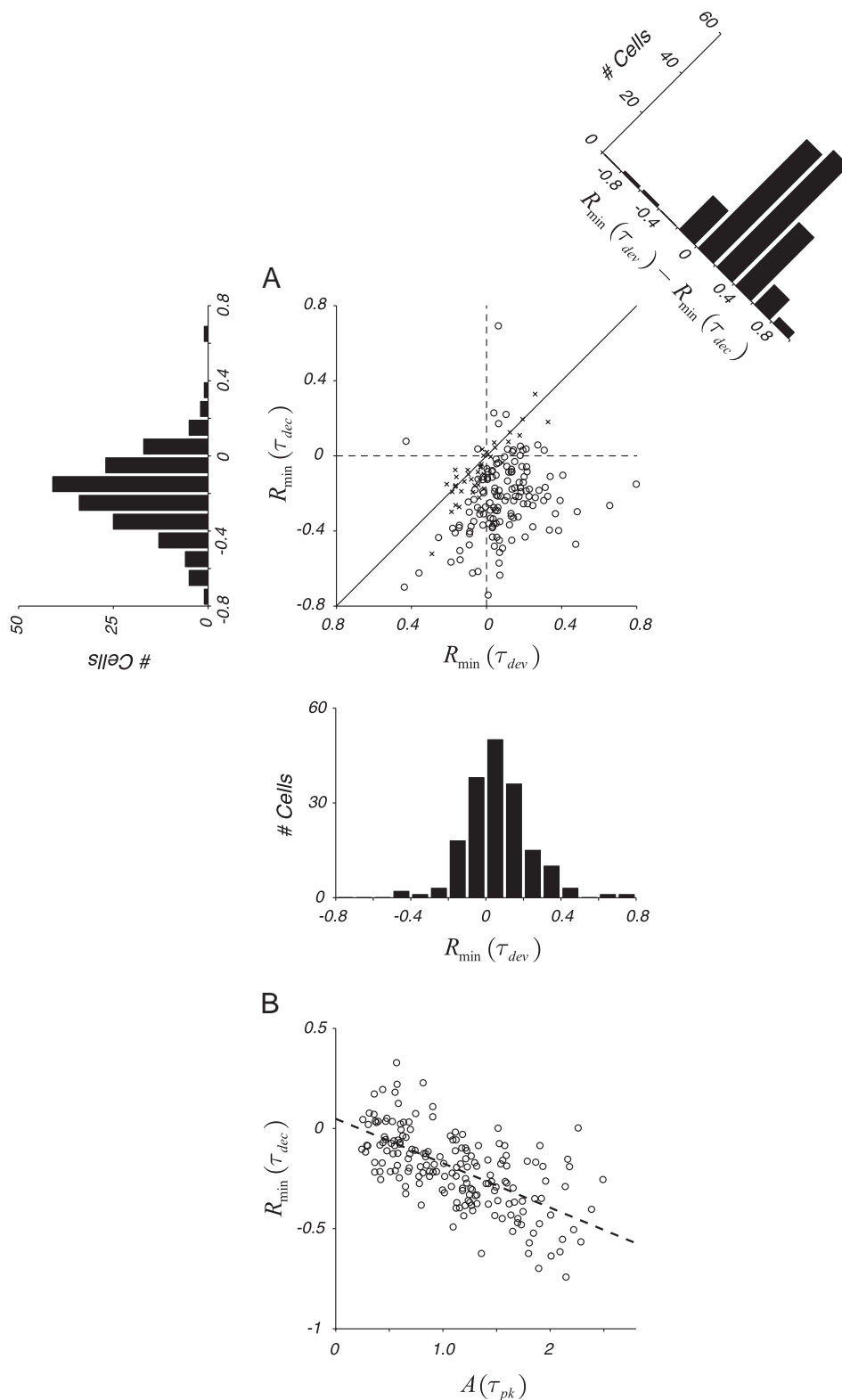


FIG. 4. Population analysis of the dynamics of the minimum response, R_{\min} . *A*: scatter plot of $R_{\min}(\tau_{dev})$ vs. $R_{\min}(\tau_{dec})$. ○, points for which $R_{\min}(\tau_{dev}) - R_{\min}(\tau_{dec})$ is significantly different than 0; x, statistically insignificant changes. *B*: scatter plot of the modulation depth of the tuning curve at its peak, $A(\tau_{pk})$, vs. the minimum response during response decay, $R_{\min}(\tau_{dec})$.

10^{-10}). These results on the dynamics of $R_{\min}(\tau)$ depend on being able to have a baseline against which to measure the early enhancement and later suppression. They indicate a major qualitative change in orientation-tuning curves with time across the V1 population of the kind seen in the representative neurons in Fig. 2.

It is possible to establish a correlation between orientation

selectivity and suppression by examining the natural variability across the V1 population. There is a correlation between the maximum modulation depth $A(\tau_{pk})$ and $R_{\min}(\tau_{dec})$ (Fig. 4*B*). The larger the suppression observed during response decay, the larger the modulation depth of the tuning curves at their peak. This result indicates that cortical suppression may be needed for high orientation selectivity in V1.

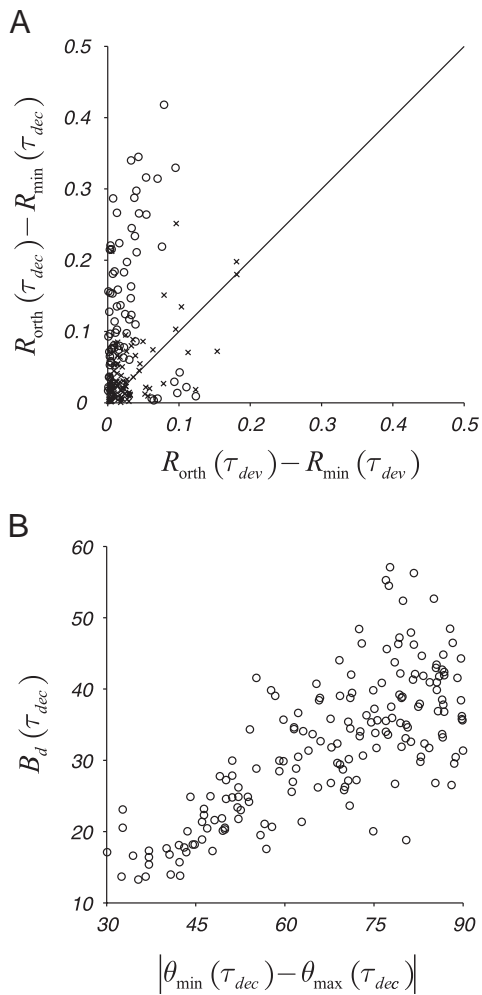


FIG. 5. Dynamical changes in the shape of the orientation tuning curves. *A*: scatter plot of the difference $R_{\text{orth}} - R_{\text{min}}$ at the development and decay of the response. Many cells during the decay have $R_{\text{orth}} - R_{\text{min}} > 0$, implying that the minimum response occurs at a location other than the orthogonal—which implies a Mexican-hat profile. \circ , points for which $R_{\text{orth}} - R_{\text{min}}$ differ significantly at τ_{dev} and τ_{dec} ; \times , statistically insignificant changes. *B*: scatter plot of the minimum orientation angle (relative to the peak) vs. the bandwidth of the cell during the decay phase. The smaller the bandwidth the closer to the peak the minimum angle occurs.

The shape of the tuning curves changes over the response period in many neurons (Fig. 5). A common pattern we observe is the transition from a Gaussian-like tuning curve to a Mexican-hat shaped one (Fig. 2, *C* and *D*). To quantify this effect, we compared the minimum response to the response at the orthogonal orientation. Figure 5*A* shows a scatter-plot for $R_{\text{orth}} - R_{\text{min}}$ at the development and decay times. When the minimum response in the tuning curve occurs at the orthogonal orientation, $R_{\text{orth}} - R_{\text{min}} = 0$. For a Mexican-hat shaped tuning curve, this difference will be positive, as the minimum occurs at an orientation other than the orthogonal. The population data in Fig. 5*A* show that most cells have a minimum response near the orthogonal orientation both during the development and the decay of the response but that during the decay phase, a significant number of cells have $R_{\text{orth}} > R_{\text{min}}$, implying a Mexican-hat shape for the tuning curve of these neurons.

The location of the minimum response relative to the peak orientation correlates with the bandwidth of the cell (Fig. 5*B*).

Cells that are broadly tuned tend to have their minimum response at locations near the orthogonal orientation, whereas cells that are more sharply tuned tend to have a minimal response at flanking orientations ($<90^\circ$ away). The graph in Fig. 5*B* illustrates the point that whenever the bandwidth during the decay phase was small (indicating the cell was sharply tuned), flank suppression was invariably observed.

The bandwidth can change dynamically over time (Fig. 6). A scatter-plot of $B_d(\tau_{\text{dev}})$ versus $B_d(\tau_{\text{dec}})$ shows that the bandwidths of some cells narrow (points below the unit line) and others broaden (points above the unit line; Fig. 6*A*). Figure 6*B* depicts the percent decrease in bandwidth versus the bandwidth of the tuning curve at τ_{dev} . A summary of the data is provided in the form of two histograms showing the percent decrease in bandwidth for cells that achieve a small bandwidth [$B_d(\tau_{\text{dev}}) < 30^\circ$] and those that do not [$B_d(\tau_{\text{dev}}) \geq 30^\circ$; Fig. 6*C*]. Sharply tuned cells sharpen over time (Fig. 6*C*, *top*, *t*-test, $P < 10^{-10}$) while there is a tendency for cells that are initially moderately or broadly tuned to broaden over time (Fig. 6*C*, *bottom*, *t*-test, $P < 0.015$).

To investigate if the changes in bandwidth occur preferentially during the rising or decay phase of the response, we plotted the relative change in bandwidth, as a function of the initial bandwidth, in the time periods $(\tau_{\text{dev}}, \tau_{\text{pk}})$ and $(\tau_{\text{pk}}, \tau_{\text{dec}})$ (Fig. 7). The scatter plots have the same overall structure as the one in Fig. 6*B*. Sharply tuned cells (with bandwidths $<30^\circ$) tend to show a decrease in bandwidth in both periods, with a slighter larger decrease during the decay phase (mean of 4.6% decrease in the rising phase and 6.3% in the falling phase). The situation appears to be more complex for broadly tuned cells, which also show a decrease in bandwidth during the rising phase but appear to broaden during the decay. The net effect is a slight broadening (Fig. 6, *A* and *B*).

The preferred orientation of neurons usually remained relatively constant within the $(\tau_{\text{dev}}, \tau_{\text{dec}})$ window, but significant changes in the order of 5–15° were observed in some neurons (Fig. 8). We note that the present analysis of orientation shifts was restricted to the time window defined by τ_{dev} and τ_{dec} . As reported by us previously, if we were to look at times larger than τ_{dec} , many of the tuning curves that develop into Mexican-hat profiles at τ_{dec} will evolve into a tuning curve that appears “inverted” at a later time and where the maximum is at the orthogonal orientation (Ringach et al. 1997b). We define a response to be inseparable in orientation and time if either the bandwidth or the peak orientation showed significant changes between τ_{dev} and τ_{dec} . With this criterion, 123 of 178 cells (69%) showed inseparable responses.

Model-based interpretation of orientation dynamics

The empirical results presented in Figs. 2 and 3 indicate that there are at least three different kinds of processes leading to orientation selectivity and that they overlap in time in the dynamical responses. To explore the mechanisms of suppression, we fitted a three-component model to the data. One component was tuned enhancement; one was tuned suppression; and the third component was untuned (or global) enhancement or suppression (depending on the sign of the global term). The three-component model is described by $R(\theta, \tau) = \alpha(\tau)E(\theta) + \beta(\tau)S(\theta) + \gamma(\tau)$. Here $E(\theta) > 0$ and $S(\theta) < 0$ represent tuned enhancement and suppression components, and

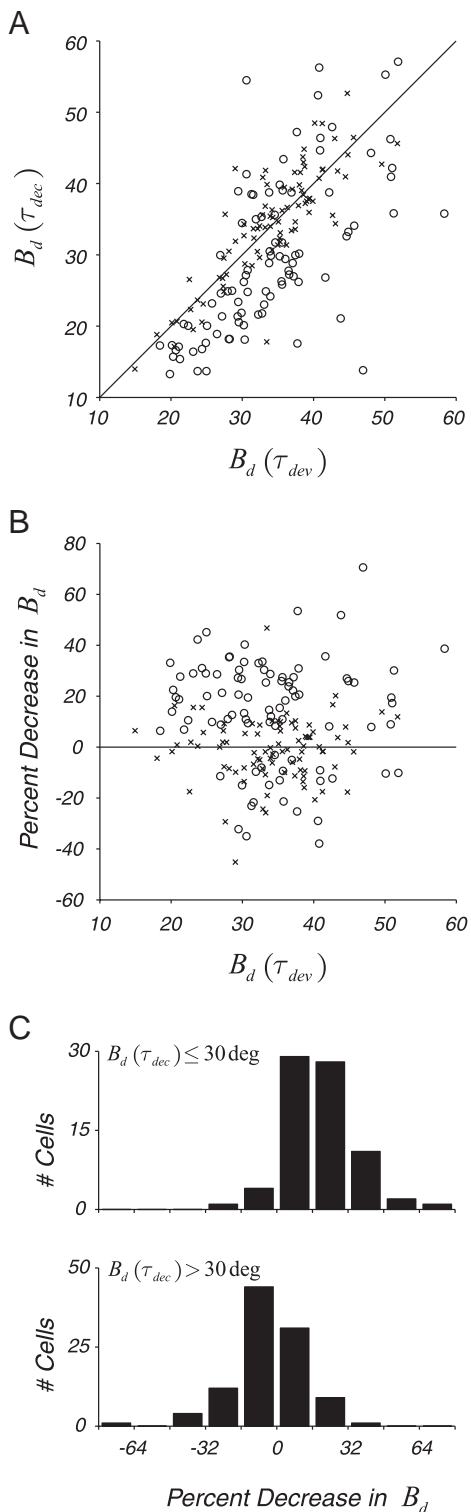


FIG. 6. Dynamical changes in bandwidth. A: scatter plot of the dynamic bandwidth at the response development and decay. Points below the unit line indicate narrowing of the cell's bandwidth, points above the unit line indicate broadening. \circ , points for which $B_d(\tau_{dec}) - B_d(\tau_{dev})$ differs significantly from 0; \times , statistically insignificant changes. B: percent decrease in bandwidth as a function of the dynamical bandwidth at τ_{dev} . C: percent change in a subset of well-tuned cells $B_d(\tau_{dec}) \leq 30^\circ$ vs. a set of broadly tuned cells $B_d(\tau_{dec}) > 30^\circ$.

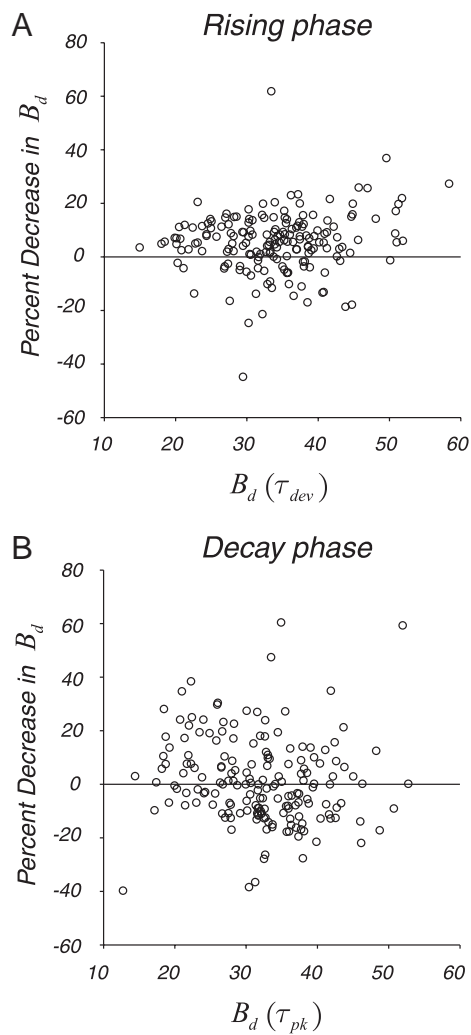


FIG. 7. Dynamical changes in bandwidth during the rising phase of the response from τ_{dev} to τ_{pk} (A) and during the decay phase of the response from τ_{pk} to τ_{dec} (B). The scatter plots show the percent decrease in bandwidth as a function of the initial bandwidth in each period.

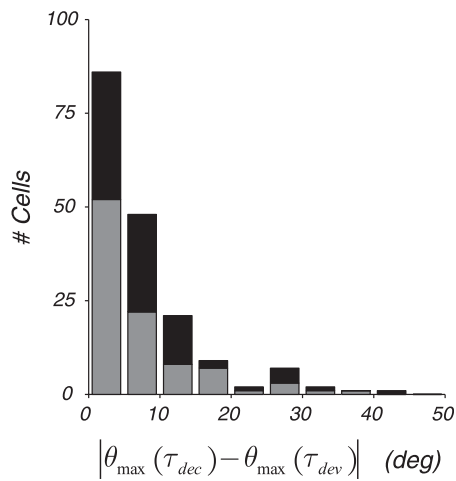


FIG. 8. Dynamic changes in preferred orientation. \blacksquare , statistically significant changes; \blacksquare , statistically insignificant changes.

their shapes are parameterized by (normalized) von Mises functions with different centers and widths (see METHODS). At each point in time, the response $R(\theta, \tau)$ is approximated as a linear combination of these two tuned components plus the flat (global) component. The coefficients $\alpha(\tau)$, $\beta(\tau)$, and $\gamma(\tau)$ represent the coefficients for tuned enhancement, tuned suppression, and the global component, respectively. While $\alpha(\tau)$ and $\beta(\tau)$ were constrained to be positive, $\gamma(\tau)$ was free to be either positive or negative. The model provided very good fits to the data (in 90% of the neurons the residual variance was $<10\%$). Figure 9A shows an example of how dynamics data in Fig. 2D (open circles) were fit by the model (solid curves) at τ_{dev} and τ_{dec} by linear combination of the fixed components shown right.

Global and local suppression develop during the time course of the response (Fig. 9B). We define the “strength” of each component by the area under it. Specifically, the area bounded between the orientation axis and $\alpha(\tau)E(\theta)$ is denoted by $\alpha(\tau)$, the area bounded by $\beta(\tau)S(\theta)$ is denoted by $\beta(\tau)$, and the area bounded by the constant component $\gamma(\tau)$. To compare the relative weight of each component, we define $\alpha'(\tau) = \alpha(\tau)/(\alpha(\tau) + \beta(\tau) + |\gamma(\tau)|)$, $\beta'(\tau) = \beta(\tau)/(\alpha(\tau) + \beta(\tau) + |\gamma(\tau)|)$ and $\gamma'(\tau) = \gamma(\tau)/(\alpha(\tau) + \beta(\tau) + |\gamma(\tau)|)$. Notice that α' and β' are always positive but that γ' can be either positive or negative. Because $\alpha' + \beta' + |\gamma'| = 1$, we can visualize the points (α' , β' , γ') in barycentric coordinates (Fig. 9B). The coordinates of each point are graphed as distance from the sides of two abutting equilateral triangles. Distance from the right hand side of each triangle is the relative weight of tuned enhancement, α' . Distance from the left hand side is the relative weight of tuned suppression, β' . Distance above and below the common base of the triangles is the signed weight of the global component, γ' (if γ' is positive the point is plotted in the upper triangle, if it is negative in the lower triangle).

Figure 9B, left, shows that the responses at τ_{dev} are mainly

located in the upper triangle near the left-hand side. This implies that average relative weight of tuned enhancement, $\alpha'(\tau_{dev})$, was much greater than the weight of tuned suppression, $\beta'(\tau_{dev})$, and the global component was net positive—meaning global enhancement was fairly strong in most cells at τ_{dev} . Relative to the distribution of points at τ_{dev} , the distribution of the relative component weights later in the response, at τ_{dec} , is shifted down and to the right (Fig. 9B, right). The shift downward implies that, during the decay phase, the global component’s sign $\gamma'(\tau_{dec})$ shifts from positive to negative; the shift rightward implies that a tuned suppressive component must be included to fit the tuning curves at τ_{dec} . Early in the response, the tuned suppressive component is weaker than the enhancement component (points clustered to the left of the diagram). But later, tuned suppression and enhancement are more nearly equal (points near the vertical axis of the diamond).

The modeling also reveals that global suppression grows stronger with time, and for many neurons is also comparable in strength to tuned enhancement—as seen by the cluster of neurons that lie near the middle of the lower triangle in the right-hand barycentric plot of Fig. 9B. Furthermore the results show that the relative strengths of tuned enhancement, tuned suppression, and global enhancement and suppression vary dynamically. Within this model, the changes in bandwidth, the development of Mexican-hat profiles, and changes in preferred orientation are explained by the development of the tuned suppressive component over time. Although in some cases the suppression may appear smaller than the enhancement in the plots of $R(\theta)$, this does not mean necessarily that the neural mechanisms of suppression are weak. Overlap in time and orientation of enhancement and suppression can mask the true strength of the suppressive signals. The results of the descriptive model presented in Fig. 9 support this reasoning.

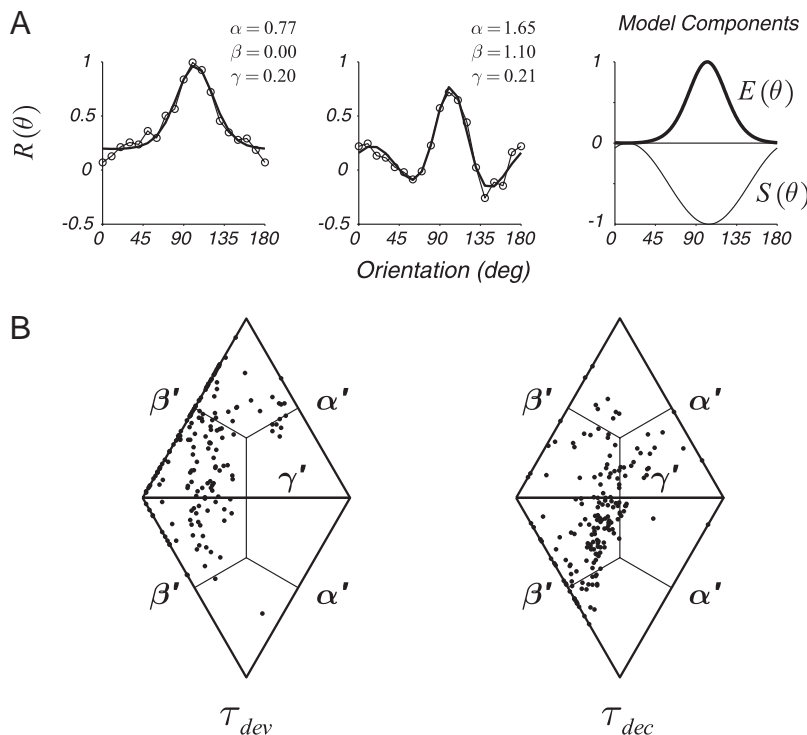


FIG. 9. Model-based interpretation of orientation tuning dynamics. A, left and middle: the data in Fig. 2D (middle) and the corresponding fits (solid lines) of a 3-component model having a tuned enhancement component (right, solid line), a tuned suppressive component (right, thin line), and a constant (global) component. Each of the curves on the left and middle are obtained as a linear combination of these left and middle components with the coefficients listed at the inset. B: relative strength of the components in the population at τ_{dev} and τ_{dec} .

DISCUSSION

We re-examined the dynamics of orientation tuning using a modification of the reverse-correlation method that permits the detection of global enhancement and suppression. This is an advantage over previous methods that only yield, at each time lag, the relative probability of firing for each orientation. Using this older methodology, we *indirectly* inferred the presence of a tuned suppressive component based on the changes in shape of the probability $p(\theta, \tau)$ (Ringach et al. 1997b). The present technique makes global and tuned suppression evident by the inclusion of “blank” images in the sequence. Both global and tuned suppression contribute to the development of orientation selectivity by enhancing the overall “modulation depth” of the tuning curve. In addition, tuned suppression is responsible for dynamic decreases in orientation bandwidth and for the generation of Mexican-hat-shaped tuning profiles, especially in cells that are very well tuned. These results are in general agreement with two recent reports from our group that showed the association of suppression and tuning selectivity using a different kind of dynamical stimuli (Ringach et al. 2002a) and the diversity of steady-state orientation selectivity and the association of high selectivity with suppression below spontaneous firing at off-peak locations (Ringach et al. 2002b). All of these recent results, together with previous work (Benevento et al. 1972; Blakemore and Tobin 1972; Bonds 1989; Crook et al. 1997, 1998; Monier et al. 2000; Nelson 1991; Nelson and Frost 1978; Pei et al. 1994; Sato et al. 1986; Sillito et al. 1980), point to the important role of suppression in generating high selectivity for orientation angle.

The results of these experiments indicate that orientation tuning in V1 is a dynamic process driven by rapid excitation and sculpted by almost equally rapid inhibitory processes. The early broad excitation that could be caused by LGN input is expected on theoretical grounds to show a response at all orientations (McLaughlin et al. 2000; Troyer et al. 1998, 2002; Wielaard et al. 2001). Our experimental data are consistent with this theoretical prediction as evident in the presence of early enhancement at all orientations. A number of investigators have proposed that this global excitation from the LGN must be cancelled, later in time, by intra-cortical inhibition to obtain sharp tuning (McLaughlin et al. 2000; Shelley et al. 2002; Troyer et al. 1998, 2002; Wielaard et al. 2001). Our results also support the notion of such a “canceling” process. However, detailed cortical network models have so far only accounted for global inhibition that would suppress the responses at all angles including the orthogonal. Tuned suppression, of the kind we have observed causes narrowing of bandwidth in the most highly tuned cells, has not been accounted for in these models yet but has been incorporated in more abstract “ring models” (Ben-Yishai et al. 1995; Carandini and Ringach 1997; Pugh et al. 2000; Somers et al. 1995). Future theoretical research has as a challenge to explain how tuned suppression arises in a model based on a realistic cortical architecture.

Comparison with results of previous studies

Gillespie et al. (2001) studied the dynamics of orientation tuning of the membrane potential in 20 cells of cat area 17. The behavior of their offset parameter [which is analogous to our global component $\gamma(\tau)$] showed an early depolarization and a

late hyperpolarization that is consistent with the global effects that we find (Fig. 9). Thus global excitation and inhibition are evident in their intracellular data. However Gillespie et al. (2001) did not observe the dynamic changes in bandwidth and preferred orientation that we observed. One major methodological difference that could explain the differences in results is that their stimuli were flashed at a relatively low temporal frequency (10 Hz); this means that the orientation of the pattern in their stimuli change every 100 ms. Because the orientation is constant throughout the integration time of the neurons, the response of the cell will represent an integrated response—or “step response”—to the constant presence of the stimulus. In contrast, if the orientations change on a faster time scale than the integration time of the cell, the result of the experiment will represent the “impulse response” of the cell to a briefly flashed orientation. We believe most of the features we observe at late times in our impulse response data are likely to be blurred by time averaging, which is what effectively is done by calculating a step response. Another important methodological difference is stimulus size. Gillespie et al. (2001) used small stimuli restricted to the “classical RF” of the cell, while we used stimuli that were two to four times the size of the RF. It is possible that some of the suppressive effects we observe originate in the surround; this means they would have not been present when stimulating with small stimuli.

Mazer et al. (2002) measured the dynamics of orientation and spatial frequency tuning of single neurons in awake, fixating monkeys using methods similar to those in our 1997 paper (see also, Bredfeldt and Ringach 2002; Ringach et al. 1997c). Their stimuli did not include blanks within the sequence and, therefore, Mazer et al. could not have measured the dynamically changing global effects (early global enhancement and later global suppression) we describe in the present paper. To address the issue of dynamic changes in the shape of the tuning curve, Mazer et al. (2002) applied a singular value decomposition (SVD) of $p(\theta, \tau)$ and calculated the amount of variance accounted for by the first component. Their data were described as being largely separable in orientation/time and spatial-frequency/time because a single component could account for a large percentage (~90%) of the overall variance. Separability in orientation/time means that there are no dynamical changes in the shape of the tuning curve. A possible reason for this discrepancy is that an SVD analysis will be mainly dominated by the large values of $p(\theta, \tau)$ and any possible changes in the small probabilities at off-optimal orientations will be largely ignored. We performed a SVD analysis of $p(\theta, \tau)$ in some of the cells that showed large and statistically significant changes in our population. We assume that the minimum response across all orientations was subtracted for each time slice before the SVD calculation was performed. Even when changes were obvious, such as the cell in Fig. 2D, the amount of variance accounted for by a single component was large (93% in this case). Thus we think that because the variance of the signal in $p(\theta, \tau)$ is dominated strongly by the central peak, the SVD analysis might not be sensitive enough to detect clear geometric changes in the shape of the tuning curve that, nevertheless, contribute moderately to the overall energy of the signal. Our analysis, instead, is based on the logarithm of the probability, which will tend to emphasize the structure of the tuning curve at off-peak locations. Therefore the differences between our results and those of Mazer et al.

are likely due to the combination of insensitivity of their analysis method and a low signal to noise in their data.

Mazer et al. (2002) also criticized our previous work stating that the dynamical features we observed could have been caused by temporal smoothing of noise because of the temporal autocorrelation of the frames, that artifacts can arise when calculating cross-correlations at 1-ms time scales, that the statistical significance of the smoothed data cannot be assessed, and that our normalization of the distribution of spikes counts across bins is inappropriate. We answer these criticisms as follows. First, the stimulus is not a constant frame that changes instantaneously from one pattern to the next in the sequence. In a typical situation, the entire computer screen, at a viewing distance of 114 cm, spans $\sim 15^\circ$ of visual angle in both vertical and horizontal axes. The size of a typical receptive field in parafoveal V1 is $\sim 1^\circ$ in diameter. Thus it takes the raster < 2 ms to stimulate the area corresponding to the RF. From the point of view of the cell, the stimulus resembles a sequence of short pulses with no stimulation in between. The autocorrelation of the input is then a very sharp peak ~ 3 ms wide and can be considered effectively white—there are no long temporal autocorrelations in the stimulus as Mazer et al. (2002) suggest. Nevertheless, our data are indeed smoothed in time with a box window of width T . This is a consequence of the algorithm used, which assigns a spike to the orientation that was presented last when looking back τ ms into the stimulus. This smoothing was done to increase the signal to noise of the measurements at the expense of losing some temporal resolution. Smoothing will only blur any features present in the data and cannot create new ones. Clearly a Mexican-hat profile cannot be generated by smoothing a family of Gaussian-shaped tuning curves. Mazer et al. (2002) also suggested that a smooth change in the preferred orientation may result simply from temporal smoothing of a noisy signal. This is indeed correct and can happen if the total number of spikes to be distributed in the orientation bins is small. However, the statistical significance of such a shift can be assessed in the way we propose here using bootstrapping methods and our data show statistically significant shifts in many cells. Finally, we do not think there is any difference in the normalization procedure used by us versus that used by Mazer et al. Each time slice in our data gets normalized by the same number, which also corresponds to a simple scaling operation as in Mazer et al. (2002) (see METHODS). We also point out that scaling of the data is irrelevant for the analysis in the present study that is based on the ratio between the tuning curve at one orientation and a blank. Scaling, as long as it is identical at each time frame, will not change any of the results reported here.

In another recent study, Sharon and Grinvald measured the average dynamics of orientation tuning in cat area 17 using optical imaging with voltage-sensitive dyes (Sharon and Grinvald 2002). Similar to the findings of Gillespie et al. (2001), these authors report the “step response” of the optical signal and found no major changes in its bandwidth during the time course of the response. They interpreted their results as implying that the bandwidth of orientation tuned neurons in V1 was constant with time. However, given the data presented here and the preceding considerations about step-response measurements, it is likely that Sharon and Grinvald could not have resolved the sharpening in bandwidth we observed. Also, it is important to realize that narrowing of the orientation band-

width does not occur in every cell but tends to be most prominent in sharply tuned neurons (Fig. 6C), which are a minority of the population. Second, broadening (of the tuning curves of more broadly tuned neurons) is also seen in our data (Fig. 6C). This suggests that the optical signal, which represents an average of the population, might have missed the effects seen when recording individual neurons.

Two other groups have measured the step response of macaque V1 neurons to a flashed bar or grating at different orientations and built dynamical orientation tuning curves by temporal slicing of these data (Celebrini et al. 1993; Muller et al. 2001). In examples shown by Celebrini et al. (1993), there is evidence of fast suppression at off-optimal orientation, which is consistent with our results. We think the failure of both groups to observe dynamic changes in bandwidth could be due to the coarser time resolution of their measurements (10 and 50 ms, respectively) and the fact that they are analyzing step responses and not impulse responses. Furthermore, in some cells, threshold effects (flashing gratings when the spontaneous firing rate of the cell is near or at 0) probably prevented the measurement of subthreshold orientation tuning dynamics. Celebrini et al. (1993) interpreted the fast emergence of a well-tuned response as evidence for a feed-forward theory of orientation selectivity. However, this interpretation was based on the assumption that intracortical inhibition is a slow process, taking hundreds of milliseconds, contrary to the evidence we supply here and to their own published examples. In addition, recent theoretical work (Jin and Seung 2002) shows that in the context of a cortical network model with rapid inhibition, one should actually expect the fast emergence of a tuned response.

This work was supported by National Eye Institute Grants EY-12816 to D. L. Ringach, EY-08300 to M. J. Hawken, EY-01472 to R. M. Shapley, a core grant P30-EY-130709 to New York University, and a Research to Prevent Blindness grant to the Jules Stein Eye Institute at UCLA.

REFERENCES

- Ben-Yishai R, Bar-Or RL, and Sompolinsky H.** Theory of orientation tuning in visual cortex. *Proc Natl Acad Sci USA* 92: 3844–3848, 1995.
- Benevento LA, Creutzfeldt OD, and Kuhnt U.** Significance of intracortical inhibition in the visual cortex. *Nat New Biol* 238: 124–126, 1972.
- Blakemore C and Tobin EA.** Lateral inhibition between orientation detectors in the cat's visual cortex. *Exp Brain Res* 15: 439–440, 1972.
- Bonds AB.** Role of inhibition in the specification of orientation selectivity of cells in the cat striate cortex. *Vis Neurosci* 2: 41–55, 1989.
- Bredfeldt CE and Ringach DL.** Dynamics of spatial frequency tuning in macaque V1. *J Neurosci* 22: 1976–1984, 2002.
- Carandini M and Ringach DL.** Predictions of a recurrent model of orientation selectivity. *Vision Res* 37: 3061–3071, 1997.
- Celebrini S, Thorpe S, Trotter Y, and Imbert M.** Dynamics of orientation coding in area V1 of the awake primate. *Vis Neurosci* 10: 811–825, 1993.
- Crook JM, Kisvarday ZF, and Eysel UT.** GABA-induced inactivation of functionally characterized sites in cat striate cortex: effects on orientation tuning and direction selectivity. *Vis Neurosci* 14: 141–158, 1997.
- Crook JM, Kisvarday ZF, and Eysel UT.** Evidence for a contribution of lateral inhibition to orientation tuning and direction selectivity in cat visual cortex: reversible inactivation of functionally characterized sites combined with neuroanatomical tracing techniques. *Eur J Neurosci* 10: 2056–2075, 1998.
- Efron B and Tibshirani RJ.** *An Introduction to the Bootstrap*. New York: Chapman & Hall, 1993.
- Gillespie DC, Lampl I, Anderson JS, and Ferster D.** Dynamics of the orientation-tuned membrane potential response in cat primary visual cortex. *Nat Neurosci* 4: 1014–1019, 2001.

- Jin DZ and Seung HS.** Fast computation with spikes in a recurrent neural network. *Phys Rev E Stat Nonlin Soft Matter Phys* 65: 051922, 2002.
- Mardia KV.** *Statistics of Directional Data*. London, UK: Academic, 1972.
- Mazer JA, Vinje WE, McDermott J, Schiller PH, and Gallant JL.** Spatial frequency and orientation tuning dynamics in area V1. *Proc Natl Acad Sci USA* 99: 1645–1650, 2002.
- McLaughlin D, Shapley R, Shelley M, and Wiesel DJ.** A neuronal network model of macaque primary visual cortex (V1): orientation selectivity and dynamics in the input layer 4Calpha. *Proc Natl Acad Sci USA* 97: 8087–8092, 2000.
- Monier C, Chavane F, Baudot P, Borg-Graham L, and Fregnac Y.** Direct evidence for a role of inhibition in orientation and direction selectivity in V1 neurons. *Soc Neurosci Abstr* 26: 139, 2000.
- Muller JR, Metha AB, Krauskopf J, and Lennie P.** Information conveyed by onset transients in responses of striate cortical neurons. *J Neurosci* 21: 6978–6990, 2001.
- Nelson JI and Frost BJ.** Orientation-selective inhibition from beyond the classic visual receptive field. *Brain Res* 139: 359–365, 1978.
- Nelson SB.** Temporal interactions in the cat visual system. I. Orientation-selective suppression in the visual cortex. *J Neurosci* 11: 344–356, 1991.
- Pei X, Vidyasagar TR, Volgushev M, and Creutzfeldt OD.** Receptive field analysis and orientation selectivity of postsynaptic potentials of simple cells in cat visual cortex. *J Neurosci* 14: 7130–7140, 1994.
- Pugh MC, Ringach DL, Shapley R, and Shelley MJ.** Computational modeling of orientation tuning dynamics in monkey primary visual cortex. *J Comput Neurosci* 8: 143–159, 2000.
- Ringach DL, Bredfeldt CE, Shapley RM, and Hawken MJ.** Suppression of neural responses to nonoptimal stimuli correlates with tuning selectivity in macaque V1. *J Neurophysiol* 87: 1018–1027, 2002a.
- Ringach DL, Hawken MJ, and Shapley R.** Dynamics of excitatory and inhibitory mechanisms shaping orientation tuning of neurons in V1. *Soc Neurosci Abstr* 23: 1544, 1997a.
- Ringach DL, Hawken MJ, and Shapley R.** Dynamics of orientation tuning in macaque primary visual cortex. *Nature* 387: 281–284, 1997b.
- Ringach DL, Sapiro G, and Shapley R.** A subspace reverse-correlation technique for the study of visual neurons. *Vision Res* 37: 2455–2464, 1997c.
- Ringach DL, Shapley RM, and Hawken MJ.** Orientation selectivity in macaque V1: diversity and laminar dependence. *J Neurosci* 22: 5639–5651, 2002b.
- Sato H, Katsuyama N, Tamura H, Hata Y, and Tsumoto T.** Mechanisms underlying orientation selectivity of neurons in the primary visual cortex of the macaque. *J Physiol* 494: 757–771, 1986.
- Sceniak MP, Ringach DL, Hawken MJ, and Shapley R.** Contrast's effect on spatial summation by macaque V1 neurons. *Nat Neurosci* 2: 733–739, 1999.
- Sharon D and Grinvald A.** Dynamics and constancy in cortical spatiotemporal patterns of orientation processing. *Science* 295: 512–515, 2002.
- Shelley M, McLaughlin D, Shapley R, and Wiesel DJ.** States of high conductance in a large-scale model of the visual cortex. *J Comput Neurosci* 13: 93–109, 2002.
- Sillito AM, Kemp JA, Milson JA, and Berardi N.** A re-evaluation of the mechanisms underlying simple cell orientation selectivity. *Brain Res* 194: 517–520, 1980.
- Somers DC, Nelson SB, and Sur M.** An emergent model of orientation selectivity in cat visual cortical simple cells. *J Neurosci* 15: 5448–5465, 1995.
- Swindale NV.** Orientation tuning curves: empirical description and estimation of parameters. *Biol Cybern* 78: 45–56, 1998.
- Troyer TW, Krukowski AE, and Miller KD.** LGN input to simple cells and contrast-invariant orientation tuning: an analysis. *J Neurophysiol* 87: 2741–2752, 2002.
- Troyer TW, Krukowski AE, Priebe NJ, and Miller KD.** Contrast-invariant orientation tuning in cat visual cortex: thalamocortical input tuning and correlation-based intracortical connectivity. *J Neurosci* 18: 5908–5927, 1998.
- Volgushev M, Vidyasagar TR, and Pei X.** Dynamics of the orientation tuning of postsynaptic potentials in the cat visual cortex. *Vis Neurosci* 12: 621–628, 1995.
- Wiesel DJ, Shelley M, McLaughlin D, and Shapley R.** How simple cells are made in a nonlinear network model of the visual cortex. *J Neurosci* 21: 5203–5211, 2001.